Trop J Nat Prod Res, January 2026; 10(1): 6758 – 6772

ISSN 2616-0684 (Print)
ISSN 2616-0692 (Electronic)

Tropical Journal of Natural Product Research

Available online at https://www.tjnpr.org

Original Research Article

Bromopyrrole Alkaloid Stevensines as Potent, Dual-Mechanism Antifouling Agents Targeting GSK-3*β* and Acetylcholinesterase

Walter Balansa[1]*, Riyanti[2], Jelita S.H. Hinonaung[3], Kirsten H. Balansa[4], Frets J. Rieuwpassa[1], Revolson A. Mege[5]

[1]*Department of Fisheries and Maritime Technology, Politeknik Negeri Nusa Utara, North Sulawesi 95811, Indonesia*
[2]*Faculty of Fisheries and Marine Science, Universitas Jenderal Soedirman. Jl. Dr. Soeparno, Banyumas 53122, Central Java, Indonesia*
[3]*Department of Health, Politeknik Negeri Nusa Utara, North Sulawesi 95811, Indonesia*
[4]*Department of Informatics Engineering, Faculty of Engineering, Universitas Sam Ratulangi. Manado 95115, North Sulawesi, Indonesia*
[5]*Biology Department, Faculty of Mathematics, Natural and Earth Sciences, Manado State University, Tondano, 95619, Indonesia*

ARTICLE INFO

Article history:
Received 03 September 2025
Revised 26 December 2025
Accepted 02 January 2026
Published online 01 February 2026

ABSTRACT

Bromopyrrole alkaloids such as hymenialdisine (**1**) and debromohymenialdisine (**2**) are recognized as potent protein kinase inhibitors and antifoulants. Despite the urgent need for novel, eco-friendly antifoulants, research on these alkaloids remains narrow, with limited understanding of their environmental fate. This study aimed to investigate the antifouling potential of a hymenialdisine analogue, stevensine, dereplicated from the Indonesian sponge *Stylissa carteri*. Preliminary antimicrobial activity of the sponge extract was evaluated using disc diffusion assay. Inspired by initial antimicrobial findings, a comprehensive in-silico investigation was conducted on stevensine and its derivatives, generated via MetaTox analysis. This involved molecular docking against multiple targets: the quorum sensing receptor (QSR), glycogen synthase kinase-3*β* (GSK-3*β*), and acetylcholinesterase (AChE). Preliminary antimicrobial activity assessment demonstrated that *S. carteri* extract inhibited the growth of the biofilm-forming bacteria *Acinetobacter baumannii* and *Staphylococcus aureus*, suggesting broad-spectrum antifouling activity. Molecular docking of stevensine and its derivatives revealed tunable scaffolds that exhibit selective inhibition towards either GSK-3*β* or AChE, potent quorum sensing, and dual- or triple-target inhibition. Statistical analysis showed significant differences in interaction energies among target groups (ANOVA, p = 0.00000832), particularly between AChE and the QSR (p = 0.0000004964) and between GSK-3*β* and the QSR (p = 0.004177242). Most importantly, predicted ecotoxicity profiles indicated that the stevensine scaffold possesses more favorable Log K_{oc}, BCF, and Log K_{ow} values than commercial antifoulants, suggesting a lower bioaccumulation potential. This study provides first evidence supporting stevensine derivatives as a versatile, multi-stage antifouling agents, positioning them as promising leads for the design of ecofriendly antifoulants.

Keywords: Eco-friendly, Antifoulants, Stevensine alkaloids, Computational study.

Introduction

The search for ecofriendly and sustainable antifoulants has increasingly focused on marine organisms-derived metabolites.[1–7] Among these, the bromopyrrole alkaloids, a diverse class of metabolites isolated from a few species of marine sponges, represent exceptionally promising yet underexplored antifouling candidates. Early studies have demonstrated that oroidin-derived alkaloids such as hymenialdisine (**1**), debromohymenialdisine (**2**), stevensine (**3**), and axinohydantoin exhibit various bioactivities (e.g., anti-cancer, anti-inflammatory, neuroprotective, and antifouling) agents.[8] The molecular basis for this broad activity is their shared pyrrolo[2,3-c]azepin-8-one core, which functions as a privileged scaffold for the potent inhibition of therapeutically important kinases like CDKs and GSK-3*β* and for antifouling activity.[8]

*Corresponding author. Email: walter.balansa@fulbrightmail.org
Tel: +6282190626822

Citation: Balansa W, Riyanti, Hinonaung JSH, Balansa KH, Rieuwpassa FJ, Mege RA. Bromopyrrole Alkaloid Stevensines as Potent, Dual-Mechanism Antifouling Agents Targeting GSK-3*β* and Acetylcholinesterase. Trop J Nat Prod Res. 2026; 10(1): 6758 – 6772 https://doi.org/10.26538/tjnpr/v10i1.46

Official Journal of Natural Product Research Group, Faculty of Pharmacy, University of Benin, Benin City, Nigeria

The established ability of these alkaloids to modulate fundamental cellular signaling pathways provides a compelling, mechanistically-driven rationale for their potential as antifouling agents.[8] This concept is supported by our previous research on the triterpene saponin sarasinosides,[9] in which, it was argued that the antifouling effect of sarasinosides, once attributed solely to antimicrobial properties,[10] is more likely rooted in their ability to disrupt core cholinergic signaling pathways, such as those mediated by Rap GTPase, which are also known to drive cancer progression.[11,12] This indicates a broader principle, indicating that natural products that inhibit fundamental cellular processes often possess multiple potent bioactivities, including anticancer and antifouling effects.[8]

Therefore, bromopyrrole alkaloids such as hymenialdisine and debromohymenialdisine represent exceptionally strong candidates for detailed investigation as antifoulants. Their well-documented roles as potent kinase inhibitors and antifouling agents suggest they may operate through novel antifouling mechanisms.[8, 13] Indeed, kinase cascades are essential for regulating the larval attachment and metamorphosis of fouling invertebrates, particularly those involving enzymes like GSK-3β.[14] Inhibition of these pathways can arrest larval development and prevent their successful settlement.[14] As mentioned earlier, both potent kinase inhibitors, hymenialdisine and its debromo-analogue, have been identified as natural antifouling compounds in their host sponge, *Axinella* sp.[13]

Despite this strong mechanistic foundation and direct ecological evidence, the antifouling potential of many structurally related bromopyrrole alkaloids has been overlooked. A good example is

stevensine, an alkaloid that features the same pyrrolo[2,3-c]azepin-8-one core but has primarily been characterized for its antifeedant properties against the fish *Thalassoma bifasciatum*,[15] and its antibacterial activity against the fouling bacterium *Deleya marina*.[16] However, its capacity to deter the settlement of invertebrate larvae remains unknown. Importantly, stevensine (**3**) and the related alkaloid hymenialdisine (**1**) were recently shown to be potent inhibitors of acetylcholinesterase (AChE).[17] While AChE is a well-known target for Alzheimer's disease, it has also emerged as a key target for antifouling agents,[2,4,9,18] providing yet another compelling reason to evaluate stevensine's antifouling properties. This study aimed to bridge this knowledge gap. By analyzing antifouling extracts of the sponge *Axinella corrugata* from Siau Island, North Sulawesi, Indonesia, generating analogues of its constituent bromopyrrole alkaloid stevensine through MetaTox study and conducting molecular docking using PyRx[19] as well as environmental prediction of the studied molecules using EPI Suite™,[20] will provide the first direct evaluation of their antifouling efficacy. Ultimately, the study seeks to connect the chemical profiles of these analogues to a potent mechanism of action based on the inhibition of both kinases and AChE.

Materials and Methods

Sample collection

The marine sponge was collected by hand from a depth of **10**–**16** meters at a Seaport in Ulu Siau, North Sulawesi, Indonesia (GPS Coordinates: 2°43′53.4″ N, 125°24′42.8″ E) on June 2019. Immediately after collection, the specimens were rinsed with sterile seawater to remove sediment and debris, placed on ice, and transported to the laboratory, where they were further cleaned, and their wet weight determined. The samples were stored at -16°C prior to extraction.

Taxonomic identification

The specimen is putatively assigned to *Stylissa carteri* (Dendy, 1889) based on its characteristic flabellate, leaf-like growth form, conulose surface, and distinctive chromogenic shift from orange in situ to reddish upon atmospheric exposure (Figure 1A). While the macro-morphology is highly congruent with *S. carteri*, the recorded megasclere dimensions (styles: 167.5 x 6.09-8.90 µm) (Figure 1B) are considerably smaller than the standard diagnostic range (320-700 µm) typically reported for this species.[21] These measurements were obtained via Binocular Light Microscopy (BLM), a technique previously validated against SEM and TLM standards.[22] Given the reliability of the technique, the specimen is categorized as a small-spiculed morphotype from Siau Port, North Sulawesi. However, this assignment remains tentative pending molecular analysis to determine if these dimensions represent extreme regional variation or a distinct cryptic lineage within the family Scopalinidae.

Extraction of Stylissa carteri

The frozen sponge tissue (200 g) was thawed and macerated in methanol (150 mL). The resulting methanol extract was filtered and concentrated under reduced pressure using the same technique we reported earlier[21]. For the antimicrobial assays, 1.1 g of the dry extract was diluted in methanol to a final concentration of 10 mg/mL. The resulting stock was maintained at 4°C for future use.

Test bacteria and antibacterial evaluation

The antibacterial activity of the extract was evaluated using the disc diffusion assay as previously described by Balansa *et al*. (2020).[21] The test organisms; *Staphylococcus aureus* (ATCC 25923) and *Acinetobacter baumannii* (ATCC 19606), were sourced from the American Type Culture Collection. Each bacterium was cultured on appropriate growth medium: *S. aureus* on Nutrient Agar containing 1% BHI broth, and *A. baumannii* on Nutrient Agar with 1% marine broth. After streaking the bacteria onto the respective media, the plates were incubated at 37ºC for two hours. To assess antibacterial activity, 20 µL of the 10 mg/mL extract and the standard antibiotic were applied to sterile 6 mm discs. Once the solvent had evaporated, the discs were transferred to the inoculated agar plates. The plates were maintained at 37°C for 12 to 24 hours, at which point the diameters of the inhibitory zones were recorded.

Molecular docking

Protein preparation

Crystal structures for 6G1U (2.85 Å resolution) and 1Q5K (1.94 Å resolution) were sourced from the RCSB Protein Data Bank (http://www.rcsb.org/pdb). Using Discovery Studio the raw PDB files were refined by eliminating water molecules and heteroatoms. After adding polar hydrogens, the structures were defined as macromolecules to prepare them for the docking simulations.[19] .

Ligand selection

Hymenialdisine (**1**), Debromohymenialdisine (**2**), Stevensine (**3**), and its derivatives (**3a – 3t**) were selected as ligands for this study. Hymenialdisine (**1**) and its debrominated derivative (**2**) have been recognized as potent antifouling agents for over a decade.[13] Surprisingly, their environmental effects remain unknown. Despite its known antifeedant activity against fish, antimicrobial activity against biofouling bacteria, and striking structural resemblance to the antifoulants **1** and **2**,[13, 15, 16] the antifouling potential of stevensine (**3**) has not been determined. Furthermore, its ability to modulate acetylcholinesterase, an emerging antifouling target, makes it a compelling candidate.[2, 4, 9, 17, 18] Hence, evaluating compound **3** and its derivatives may provide insight for the discovery of desperately needed eco-friendly antifouling agents. These considerations served as the main criteria for selecting compounds **1-3**, along with the derivatives of **3**, as the primary ligands for this study.

Ligand Preparation

Ligand preparation involved drawing structures in ChemDraw 12.0 and subsequent optimization in PyRx to produce docking-ready pdbqt files. The AutoGrid parameters were meticulously defined within the AutoDock Wizard to encapsulate the active sites of both AChE (6G1U) and GSK-3β (1Q5K), using the precise Cartesian dimensions of (65.62, 141.96, 111.63) and (71.30, 77.18, 99.11) respectively.

MetaTox analysis

The derivatives of stevensine (**3a-3t**) were generated using the MetaTox webtool. The process was initiated by obtaining the SMILES string of stevensine from PubChem. This SMILES string was copied and saved as a .cdx file, which was then uploaded to the MetaTox webtool. The prediction was run with the setting that the probability of activity (Pa) must be higher than the probability of inactivity (Pi). This generated 30 potential metabolites resulting from phase I and phase II biotransformation reactions.[22] These metabolites were then subjected to molecular docking analysis against three targets; acetylcholinesterase (AChE), glycogen synthase kinase 3 beta (GSK-3*β*), and quorum sensing receptor (QSR) to predict their potential antifouling mechanisms.

Post-docking analysis of target selectivity

To elucidate the potential for selectivity or dual-target inhibition among the synthesized compounds, a post-docking analysis was conducted. The selectivity of each derivative was quantified by calculating the difference in the predicted Gibbs free energy of binding (ΔΔG) between the two protein targets. The selectivity score was computed using the formula: $\Delta\Delta G = \Delta G(GSK3\beta) - \Delta G_{bind}(AChE)$. In this convention, a negative ΔΔG signifies a thermodynamic preference for GSK3*β*, while a positive value indicates a preference for AChE. Based on the fundamental relationship between binding energy and affinity ($\Delta G = RT \ln Ki$), where a difference of ~1.4 kcal/mol corresponds to a 10-fold difference in inhibitory potency, a stringent threshold for classification was established.[23]

Based on the established principle that a difference of approximately 1.4 kcal/mol in binding energy corresponds to a 10-fold difference in inhibitory potency at room temperature, compounds can be rigorously classified. For instance, compounds are categorized as Class I (selective) if they exhibit $|\Delta\Delta G| \geq 1.4$ kcal/mol (≥ 10-fold potency difference); Class II (Preferential) if $0.7 \leq |\Delta\Delta G| < 1.4$ kcal/mol (5 to 9-fold difference); and Class III (non-selective) if $|\Delta\Delta G| < 0.7$ kcal/mol (<5-fold difference)

.

Toxicology score
To evaluate toxicological risk, a toxicology score was calculated for each compound. This approach, a previously published method,[9] involved assessing several key endpoints: Log K_{ow}, Log K_{oc}, Log BCF/BAF, Ames toxicity, hepatotoxicity, *Tetrahymena pyriformis* toxicity, and a fathead minnow toxicity test. Predictions for these endpoints were obtained from EPI Suite and pkCSM. Each endpoint was then assigned a binary value (1 = beneficial, 0 = harmful) according to established thresholds.[9] The final Toxicology Score was derived by summing these individual binary scores.

Data visualization
The compiled toxicity data were structured into a data frame using the Pandas library in Python. A heatmap was then generated via the Seaborn library to visualize these data, representing beneficial factors in blue and harmful factors in red. This graphical representation provided a clear overview of the toxicity profile for each compound, allowing for the efficient comparison of parameters and the identification of patterns.

Statistical analysis
To evaluate the selective bioactivity of stevensine (**3**) and its derivatives (**3a-3t**) against GSK-3*β*, AChE, and Quorum Sensing, a multi-stage statistical approach was used. Initial one-way ANOVA (Excel) was used to determine if significant differences in activity exist across the three targets, indicating selectivity. One-way ANOVA were followed by post-hoc analysis to identify specific compounds and targets responsible for these differences, elucidating antifouling mechanisms across pathways like the cholinergic (AChE) and GSK-3*β*. This mechanism-based approach supports the development of eco-friendly antifoulants with known actions. Experiments for AChE and GSK-3*β* inhibition were performed in ten replicates. For toxicity assessment, the Fisher's Exact Test (GraphPad: https://www.graphpad.com/quickcalcs/contingency) was used to compare the significance of derivatives' toxicity levels by classifying activities into "beneficial" (1) depicted as green and "harmful" (0) depicted as red in a heatmap scores based on predefined criteria, offering a stringent comparison of discrete toxicity outcomes.

Results and Discussion

This study bridges the knowledge gap regarding the environmental safety and antifouling mechanisms of bromopyrrole alkaloids (**1–3**). Initial antimicrobial testing of the *Styllisa carteri* crude extract contained stevensine (**3**) revealed strong antifungal against *Septoria tritici*[24] and moderate activity against biofilm-forming bacteria *Staphylococcus aureus* and *Acinetobacter baumannii*, in which the latter pose significant maritime and industrial challenges.[25–28] Following these findings and the in-silico generation of stevensine derivatives (**3a–3t**) via MetaTox analysis, we conducted molecular docking against AChE, GSK-3*β*, and quorum sensing targets. The results demonstrate that stevensine and its derivatives exhibit potent inhibitory activity—comparable or superior to the reference inhibitors synoxalidinones A (**4**) and C (**5**) and parent antifoulants (**1–2**)—while toxicological scoring indicates a more favorable environmental profile.

Antibacterial activity of the sponge extract
This investigation commenced with an antibacterial screening of sponge extracts from Ulu Sea Port (1–16 m depth). Among these, two specimens; *Agelas nakamurai* (Ulu_13) and *Stylissa carteri* (Ulu_16) were selected for further study based on their known chemical profiles. From these sponges, agelasine and the bromopyrrole alkaloid stevensine, were previously dereplicated.[24] Although, the antifouling potential of agelasine alkaloids has been a focus of recent intensive studies,[5,7] a significant knowledge gap persists regarding the bioactivity of stevensine, hence the motivation for this targeted research.

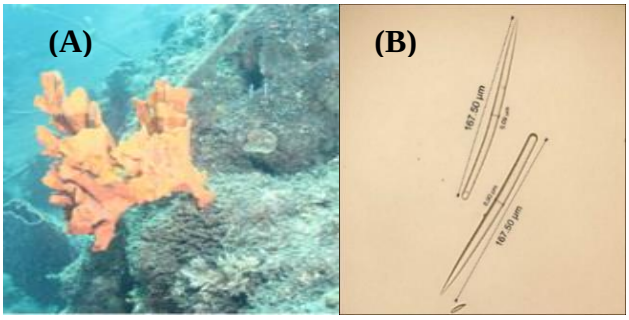

Figure 1: Morphological and spicular characteristics of *Stylissa carteri*. (A) In situ photograph of the live specimen exhibiting a flabellate growth form. (B) Light micrograph of a representative style (megasclere). The specimen was collected from a depth of approximately 12 m in Siau Port, North Sulawesi, Indonesia.

Subsequent antimicrobial tests confirmed that extracts from both sponges were capable of inhibiting key biofilm-forming pathogens, including the Gram-positive *S. aureus* and the Gram-negative *A. baumannii*. While the *S. carteri* extract (Ulu_16), containing stevensine, displayed weaker antimicrobial efficacy than the *A. nakamurai* extract (Ulu_13) (Table 1), this result does not preclude its potential as a targeted antifouling agent. Given that stevensine (**3**) is a derivative of known antifouling compounds and potent GSK-3*β* inhibitors like hymenialdisine (**1**),[13] it was posited that hymenialdisine and its derivatives (stevensine) may exert their antifouling effects through mechanisms distinct from broad-spectrum antimicrobial activity, necessitating further evaluation of their antifouling potential against the emerging and potential antifouling targets, AChE and GSK-3*β* through molecular docking.

Table 1: Antibacterial activity of methanol extract of Indonesian sponge *Styllisa carteri*

Sample	Inhibition zone diameter (mm)	
	***S.aureus* ATCC 25923**	***A. baumanii* ATCC 25923**
Ulu_13	23.83 ± 0.28 mm	20.66 ± 0.57 mm
Ulu_16	11.33 ± 0.57 mm	9.50 ± 0.50 mm
Tetracycline	25.00 ± 0.50 mm	21.00 ± 1.00 mm

Molecular docking
Molecular docking simulations revealed that hymenialdisine (**1**), debromohymenialdisine (**2**), and stevensine (**3**) are potent binders of both acetylcholinesterase (AChE) and glycogen synthase kinase 3*β* (GSK-3*β*). Compounds **1** and **2** exhibited excellent binding affinity for AChE, with binding energies of −9.06 and −9.99 kcal/mol, respectively, which exceeded those of reference inhibitor synoxalidinone A (−8.70 kcal/mol). Only compound **2** surpassed AChE inhibitor synoxalidinone C (−9.40 kcal/mol). While their affinities for GSK-3*β* were slightly lower, they remained strong at −8.09 and −8.74 kcal/mol, respectively (Table 2). These results suggest that the antifouling properties of these compounds are driven by a two-pronged mechanism involving the potent inhibition of AChE and GSK-3*β*.
Although, stevensine (**3**) exhibited a slightly weaker binding affinity than hymenialdisine (**1**) and debromohymenialdisine (**2**), it demonstrated comparable antifouling activity (Table 2). Docking simulations showed that compound **3** binds strongly to AChE (−8.17 kcal/mol) and GSK-3*β* (−8.09 kcal/mol) (Table 2). This finding not only uncovers the antifouling potential of the bromopyrrole stevensine but also confirms that it employs a two-pronged antifouling mechanism similar to that of compounds **1** and **2** with binding affinities of -8.86 and -8.74 kcal/mol for GSK-3*β* and -9.06 and -9.99 kcal/mol for AChE (Table 2).

ISSN 2616-0684 (Print)
ISSN 2616-0692 (Electronic)

Table 2: Binding affinities of antifoulants **1** and **2** along with stevensine (**3**), AChE (**4-5**), GSK-3*β* (**6-8**) inhibitors and QSR modulators (**7, 8**)

Ligand	GSK-3*β* receptor (1Q5K)	AChE (6G1U)	QSR (4K3B)
Hymenialdisine (**1**)	-8.86	-9.06	-8.84
Debromohymenialdisine (**2**)	-8.74	-9.99	-8.17
Stevensine (**3**)	-8.09	-8.17	-7.37
Synoxalidinone A (**4**)	-9.80	-8.70	-8.50
Synoxalidinone C (**5**)	-9.40	-7.80	-7.60
AZD1080 (**6**)	-9.90	-6.40	-8.40
CID_11167509 (**7**)	-11.30	-7.60	-8.80
Rosmarinic acid (**8**)	-8.90	-5.30	-7.50

Interestingly, while the reference compounds for GSK-3*β* (e.g. AZD1080, CID_11167509 and rosmarinic acid) show weak activity against AChE with binding affinities between -5.30 to -7.60 kcal/mol, the AChE inhibitors synoxalidinones A (**4**) and C (**5**) show the same broad-spectrum mechanism as the bromopyrrole hymenialdisine (**1**) and derivatives (**2**, **3**) (Table 2), extending beyond their established role as antifoulants and AChE inhibitors to include potent GSK-3*β* inhibition.[29,30] Synoxalidinone A, for instance, exhibits a remarkable –9.80 kcal/mol binding affinity for GSK-3*β*, rivaling AZD1080, despite a lower affinity for AChE (–8.70 kcal/mol). This multiple-targeting potential demonstrates a complex mode of action for the antifouling properties of synoxazolidinones A/C or stevensine derivatives.

Increasing evidence indicates that acetylcholinesterase (AChE) and GSK-3*β* are involved in various complex cellular pathways including cell signaling, including those pertinent to cancer,[31,32] suggesting that the antifouling activity of certain compounds may stem from the disruption of broader biological processes rather than solely through antimicrobial effects. This hypothesis is supported by our recent findings concerning sarasinoside structures. Their observed antifouling effects, initially attributed to antimicrobial activity,[10,33] were subsequently found to correlate with their demonstrated anticancer properties.[9] This correlation suggests that antifouling can be a manifestation of more fundamental cellular interventions, a principle that may similarly apply to the action of synoxalidinones A and C as well as stevensine.

The potent dual inhibitors, hymenialdisine (**1**) and debromohymenialdisine (**2**), demonstrate successful engagement with key catalytic residues in both target enzymes (Table 3). In Acetylcholinesterase (AChE), both compounds interact with Tryptophan 84 (Trp84), a critical residue within the catalytic anionic subsite (CAS) essential for substrate binding.[34] In contrast, despite their strong binding affinities for Glycogen Synthase Kinase-3 beta (GSK-3*β*), compounds **1** and **2** do not exhibit direct interactions with the commonly recognized ATP-binding site residues, such as Val135, Asp133, Lys85, Arg141, and Cys199.[32] Instead, their binding is localized to a distinct set of residues—Ala83, Asp131, Asp200, and Cys198 which are not typically associated with direct ATP coordination (Table 3).

Table 3: Amino acid residues of binding interactions between compounds 1-8 and GSK-3*b* (PDB ID: 1Q5K), AChE (PDB ID: 6G1U), and QSR (PDB ID: 4K3B)

Ligand	GSK-3*β* (1Q5K)	AChE (6G1U)	QSR (4K3B)
Hymenialdisine (**1**)	Ala83, Asp131, Asp200, Cys198, Cys885, Ile62, Val78	Gly117, His440, Trp84	Gly598, Val515, Leu531, Asp4 Tyr490,
Debromohymenialdisine (**2**)	Ala83, Asp133, Asp200, Cys198, Leu168, Cys885, Leu198	Asp72, Gly117, Trp84	Thr573, Asp488, Val515, Leu5 Arg516
Stevensine (**3**)	Cys199, Leu188, Ile62, Pro136, Val70	Arg289, Phe228, Phe331, Trp279,	Asn468, Asp488, Val515, Arg5
Synoxalidinone A (**4**)	Asn64, Asp264, Ser261 (hydrogen bond), Cys199 (Pi-sulfur), Ala83, Val110, Leu132, Leu188, Cys199, Ile62, Leu188, Ile62, Val70, Leu1888 (hydrophobic alkyl, pi-alkyl) (B)	Arg289, Asn230, Leu528, Pro529 Pro361	Tyr506, Phe648, Glu649, Glu5 Phe494, Val503,

Ligand	GSK-3*β* (1Q5K)	AChE (6G1U)	QSR (4K3B)
Synoxalidinone C (**5**)	Asp264, Val135, (hydrogen bond) Cys199 (Pi-sulfur), Ala83, Val110, Leu132, Leu188, Cys199, Ile62, Leu188, Val70, Leu188 (hydrophobic alkyl/Pi-alkyl) (A)	Asp285, Trp279, Trp279, (hydrogen bond), Trp279, (hydrophobic Alkyl, Pi-Pi Alkyl	Gly694, Thr508, Asp488, Try4
AZD1080 (**6**)	Ser66, Phe67, Asp264, Val70 (hydrogen bond), Leu188, val70, Ala83, Leu188, Cys199, Ile62, Ala83, Lys85, Cys199 (hydrophobic Pi-sigma/alkyl (A)	Ser24, Lys133, (hydrogen bond), (electrostatic), Leu23, Leu2 Val453 Pi-alkyl)	Thry581, Asn579, Thr581, Try Try524
CID_11167509 (**7**)	Unk1, Pro136, Gly68 (hydrogen bond), Ile62, Val70, Leu188, Cys199, Val70, Ala83, Leu188, Cys199, Ile62, Ala83 (hydrophobic Pi-sigma/alkyl (A)	Ser24, Arg467, Leu23, Leu456, Pi-sigma, Pi-alkyl (A)	Phe648, Asn650, Glu649 (hydr Tyr652, Ala499 (hydrophobic)
Rosmarinic acid (**8**)	Gln89, Glu97, Asp90 (hydrogen bond) Phe67, Pro294 (hydrophobic Pi-Pi T-shaped, Pi-alkyl	Leu23, Leu23, Unk1, Ala239 stacked, Pi-alkyl (A)	Arg459, Arg459, Arg459, Arg4 Pro476

This suggests a new and distinct mode of action, where these interactions are crucial for stabilizing an inactive conformation of GSK-3*β*, thereby effectively competing with or hindering the enzyme's normal catalytic cycle and preventing its function although this claim remained to be validated.

The GSK-3*β*-selective compounds, synoxalidinones A and C, achieve their high potency presumably through extensive and specific interactions with GSK-3*β* allosteric site. They form numerous hydrophobic contacts with residues like Ala83, Ile62, Val70, Leu132, and Leu188, and establish unique interactions such as a Pi-Sulfur bond with Cys199 (Table 3). These multiple, strong interactions anchor the molecules firmly in the GSK-3*β* pocket, explaining their high affinity. Their different structure leads to less optimal contacts within the AChE gorge, resulting in weaker binding and thus, selectivity for GSK-3*β*. These differences in binding affinity likely arise from variations in the specific amino acid interactions at the enzyme binding sites. For instance, compounds **1** and **2** interact with a common set of residues on their targets, including Ala83, Asp200, Cys198, Leu168, and Cys885. In contrast, compound **3** primarily utilizes a different set of interactions, sharing only the Ile65 residue (on GSK-3*β*) with hymenialdisine and the Phe330 residue (on AChE) with debromohymenialdisine (Table 3). This result further suggests that despite their similar two-pronged antifouling mechanisms, the three compounds, particularly compound **3**, bind differently to the active sites of both AChE and GSK-3*β*.

A closer analysis of the molecular docking poses revealed that while all three compounds target the active sites of AChE and GSK-3*β*, they do so with distinct interaction patterns particularly for stevensine. Within AChE, the active site is located in a deep gorge containing two critical regions: the Catalytic Anionic Site (CAS) and the Peripheral Anionic Site (PAS).[34] The results show that hymenialdisine (**1**) and debromohymenialdisine (**2**) firmly anchor to the PAS, a region crucial for initial ligand recognition (Table 3). This is evidenced by their key interactions with Trp84, the defining residue of the PAS, and Tyr130 and Gly117 (Table 3), similar orientation at the catalytic binding site as well as 2D amino acid residue interaction (Figure 2A and 2B). In contrast, stevensine (**3**) also binds within the active site gorge but interacts with a different set of PAS residues, including Phe330, Phe331, and Trp279, while lacking the direct interaction with Trp84 (Table 3). Additionally, its slightly different orientation at the catalytic site and amino acid residues compared to compounds **2**, **3** and AChE inhibitor (**4**) explains the different binding affinities observed for the test compounds (Figure 2, 1A-1D). This difference in binding mode within the same functional site explains how stevensine achieves potent inhibition despite having a unique molecular characteristic compared to its analogues.

A similar binding pattern was observed in the interactions between **1**-**3** and GSK-3*β* as well as between **1**-**3** and QSR. Hymenialdisine and debromohymenialdisine exhibited nearly identical binding poses, interacting with residues such as Ala83, Asp200, and Cys198 (Table 3). This high degree of overlap explains their very similar, potent binding energies. In contrast, stevensine occupied a distinct pocket within the same active site, forming interactions with different residues such as Cys199, Leu188, and Val70 (Table 3). Moreover, stevensine showed a distinct binding orientation, involving different amino acid residues in comparison to hymenialdisine, debromohymenialdisine, and synoxalidinone C (Figure 2, 2A. 2D).

These findings confirmed that while all three compounds potently target the same enzymes, they achieve their inhibitory effects through slightly different molecular mechanisms and orientations within the active sites. This result corroborates the earlier finding on the agelasine alkaloids, where the striking molecular resemblance of these alkaloids showed varying binding orientations and amino acid residues.[9,4,6] Additionally, this discovery supports modern, mechanism-based strategies in antifouling research.[35,36]

ISSN 2616-0684 (Print)
ISSN 2616-0692 (Electronic)

Although, stevensine (**3**) exhibited weaker binding affinities than hymenialdisine (**1**) and debromohymenialdisine (**2**), it remains a potent dual inhibitor of both AChE and GSK-3*β*, with binding energies of -8.17 kcal/mol and -8.09 kcal/mol, respectively. The structural analysis revealed that subtle differences in ligand-residue contacts and binding orientation, influenced by the presence and position of bromine atoms, directly correlated with the observed variations in inhibitory activity. Stevensine's known roles as an antifeedant and kinase inhibitor, coupled with recent findings on AChE inhibition as a viable antifouling strategy, provide a strong basis for its investigation as a novel antifouling agent.[15–17]

MetaTox analysis

To advance the development of next-generation antifouling compounds from the bromopyrrole scaffold, a predictive *in silico* strategy using MetaTox analysis were implemented. A similar approach applied to agelasine alkaloids led to the discovery of analogues with not only strong binding affinity towards the antifouling target AChE but also an improved ecotoxicological profile.[9] In this study, the computational study involved creating a virtual library of stevensine derivatives designed for improved target affinity. Subsequently, these candidates were subjected to molecular docking against AChE and GSK-3*β* to confirm their two-pronged mechanism. The most promising derivatives were then used for computational screening for potential ecotoxicity using EPI Suite™. This three-phase process was designed to identify potent and environmentally friendly antifouling agents, which could serve as template for the development of ecologically compatible solutions.

MetaTox analysis [22] generated a series of metabolites from the parent stevensine scaffold, resulting in an array of structurally diverse compounds for subsequent analysis. Based on a predictive threshold where potential activity (*Pa*) exceeded potential inactivity (*Pi*) or (*Pa* > *Pi*), 32 unique metabolites were generated from simulated phase I and phase II biotransformation reactions (Figures 2 and 3). Phase I metabolism was predicted to yield various oxidative products relating to the introduction of functional groups with key metabolites such as hydroxylation at multiple positions (e.g., metabolites **3b**, **3e**, **3j**), *N*-hydroxylation (**3a**), epoxidation (**3f**), and dehydrogenation (**3g**). Additionally, through conjugation reaction, phase II was predicted to yield metabolites with improved water solubility such as glucuronidated products (**3l**, **3m**, **3n** and **3o**), a sulfated product (**3p**) and a peptide like conjugation (**3c**), consistent with common metabolic pathways. For the glucuronides product in particular, this result aligns with previous results where they are the most dominant products of the phase two reactions such in the case of agelasine alkaloids.[4,9]

With the library of stevensine derivatives established, a molecular docking study was performed to assess their binding affinities against three key antifouling targets: Acetylcholinesterase (AChE; PDB ID: 6G1U), Glycogen Synthase Kinase-3*β* (GSK-3*β*; PDB ID: 1Q5K), and a Quorum Sensing Receptor (QSR; PDB ID: 4K3B). The assessment relies on the principle that a more negative free energy change (ΔG) corresponds to a more thermodynamically favorable process, such as stronger ligand-receptor binding[23]. This principle along with the compound selectivity towards the protein targets (i.e., specific or Class I, preferential or Class II and broad spectrum or Class III) is described in detail at method section of this article.

To assess the differential binding preference—or selectivity—of a compound toward two distinct protein targets (such as GSK-3β and AChE), the difference in their respective binding free energies (ΔΔG) can be calculated. As illustrated in Table 4, ΔΔG is derived by subtracting the ΔGbind of one target from the other: $\Delta\Delta G = \Delta G_{bind}(GSK\text{-}3\beta) - \Delta G_{bind}(AChE)$. A negative ΔΔG value indicates a thermodynamic preference for GSK-3β, while a positive value suggests a preference for AChE.

Table 4 shows that the stevensine scaffold inherently favors multi-target activity, with 75% of the derivatives functioning as broad-spectrum or balanced inhibitors. Specifically, compounds **1, 3d, 3e, 3f**, and **3l** are categorized as Class III (non-selective), exhibiting similar affinities across all targets, while **3, 3a**, and **3g** act as balanced dual inhibitors. In contrast, only 25% of the library demonstrates high selectivity (Class I, ΔΔG ≥ 1.4 kcal/mol), primarily favoring AChE (**3h, 3r, 3s, 3t**), with compound **3c** uniquely exhibiting a strong preference for GSK-3β. This profile represents promising candidates for developing broad-spectrum antifoulants with a multi-pronged mechanism. STV_14 (**3d**) showed high potency with nearly similar binding affinity against both targets (AChE: -9.26 kcal/mol; GSK-3*β*: -9.13 kcal/mol; ΔΔG = +0.13 kcal/mol) (Table 4). This dual activity is consistent with the known biology of the parent alkaloid, hymenialdisine, which is a powerful inhibitor of multiple kinases, including GSK-3*β*, and has been shown to block the phosphorylation of the tau protein in cellular models of Alzheimer's disease.[13, 17] The fact that AChE is not only the main target for Alzheimer's disease but has also emerged as a new target for antifouling further strengthens the idea that the interaction between AChE and GSK-3*β* inhibitors may play crucial synergistic roles in antifouling activity.

Table 4: Binding affinities of hymenialdisine (**1**), debromohymenialdisine (**2**) stevensine (**3**) and stevensine derivative (**3a-3t**)

Ligand	AChE (6G1U)	GSK3 receptor (1Q5K)	Quorum Sensing (4K3B)	ΔΔG (GSK3-AChE)	ΔΔG (QS-AChE)	ΔΔG (QS-GSK-3*β*)	Category (Primary/Secondary Preference, if any)
Hymenialdisine (**1**)	-9.06±0.77	-8.86±0.13	-8.84±0.55	0.20	0.22	0.02	Class III (Broad-Spectrum)
Debromo hymenialdisine (**2**)	-9.99±0.66	-8.74±0.51	-8.17±0.36	1.25	1.82	0.57	Class I (AChE/QS); Class II (AChE/G)
Stevensine (**3**)	-8.17±0.76	-8.09±0.40	-7.37±0.05	0.08	0.80	0.72	Class II (AChE/QS)
STV_1 **(3a)**	-8.31±0.35	-8.09± 0.49	-7.38±0.06	0.22	0.93	0.71	Class II (AChE/QS)
STV_2 (**3b**)	-8.58±0.64	-7.83±0.37	-7.38±0.06	0.75	1.20	0.45	Class II (AChE/G/QS)
STV_3 (**3c**)	-9.11±0.72	-10.14±0.86	-7.03±0.21	-1.03	2.08	3.11	Class I (GSK3/QS); Class II (G/A)
STV_4 (**3d**)	-9.21±0.98	-8.98±0.92	-8.77±0.59	0.23	0.44	0.21	Class III (Broad)
STV_5 (**3e**)	-8.67±1.02	-8.58±0.68	-8.22±0.32	0.09	0.45	0.36	Class III (Broad))
STV_6 (**3f**)	-8.08±0.61	-8.06±0.53	-7.54±0.15	0.02	0.54	0.52	Class III (Broad spectrum)
STV_7 **(3g)**	-8.32±0.94	-8.16±0.65	-7.22±0.18	0.16	1.10	0.94	Class II (AChE/QS)

STV_8 (**3h**)	-9.05±0.97	-8.25±0.49	-7.39±0.03	0.80	1.66	0.86	Class I (AChE/QS); Class II (AChE/G)
STV_9 (**3i**)	-8.34±0.73	-8.08±0.48	-7.53±0.11	0.26	0.81	0.55	Class II (AChE/QS)
STV_10 (**3l**)	-9.01±0.66	-7.79±0.38	-7.29±0.12	1.22	1.72	0.50	Class I (AChE/QS); Class II (AChE/G)
STV_11 (**3k**)	-8.22±0.31	-8.54±0.58	-7.50±0.00	-0.32	0.72	1.04	Class II (GSK3/QS)
STV_12 (**3l**)	-8.44±0.22	-8.42±0.25	-7.97±0.13	0.02	0.47	0.45	Class III (Broad)
STV_13 (**3m**)	-8.79±0.03	-8.01±0.64	-7.63±0.15	0.78	1.16	0.38	Class II (AChE/QS)
STV_14 (**3n**)	-9.26±0.10	-9.13±0.62	-7.72±0.17	0.13	1.54	1.41	Class I (AChE/QS & GSK3/QS)
STV_15 (**3o**)	-9.33±0.23	-10.0±0.78	-8.93±0.13	-0.67	0.40	1.07	Class II (GSK3/QS)
STV_16 (**3p**)	-8.20±0.36	-8.88±0.99	-8.89±0.42	-0.68	-0.69	-0.01	Class III (Broad GSK3/QS)
STV_17 (**3q**)	-8.06±0.95	-7.29±0.79	-8.09±0.28	0.77	-0.03	-0.80	Class II (AChE/G & QS/G)
STV_18 (**3r**)	-8.69±0.73	-7.27±0.40	-6.65±0.38	1.42	2.04	0.62	Class I (AChE/G/QS)
STV_19 (**3s**)	-8.77±0.84	-7.40±0.15	-6.72±0.29	1.37	2.05	0.68	Class I (AChE/QS); Class II (AChE/G)
STV_20 (**3t**)	-8.68±0.56	-7.32±0.11	-6.69±0.21	1.36	1.99	0.63	Class I (AChE/QS); Class II (AChE/G)

A one-way analysis of variance (ANOVA) was then conducted to compare the mean interaction values of the studied ligands across three distinct biological targets. They include acetylcholinesterase (AChE), a key enzyme in the nervous system, Glycogen Synthase Kinase 3 beta (GSK-3β), a serine/threonine kinase implicated in cancer and other cellular processes[37,38] and the bacterial outer membrane protein BamA, a potential antibacterial target.[39] The analysis revealed a statistically significant difference among the group means (p = 0.00000832), indicating that the ligands' interaction strength is dependent on the protein target (Table 5).

To determine the specific pairwise comparisons, a post hoc test was conducted. This involved three comparisons (k = [k-1]/2 = 3), followed by a two-sample t-test assuming unequal variance. The p-value was then adjusted using the Bonferroni correction (0.05/3), yielding a new critical p-value of 0.016666. This adjusted p-value was then compared to the results of the three t-tests. The results showed a highly significant preference for the human enzymes over the bacterial protein. Specifically, the mean difference in interaction was -1.0826087 between the AChE and 4K3B groups (p = 0.0000004964) and -0.65173913 between the GSK3β and 4K3B groups (p = 0.004177242) (Tables 6 and 7).

Table 5: Summary of ANOVA Single Factor Analysis

Groups	**Count**	**Sum**	**Average**	**Variance**		
AChE (6G1U)	23	-200.34	-8.7104	0.23756		
GSK-3β	23	-191.91	-8.3439	0.59133		
Quorum Sensing (4K3B)	23	-176.92	-7.6922	0.47856		
ANOVA						
Source of Variation	SS	Df	MS	F	p-value	F crit
Between Groups	12.2357	2	6.11784	14.0376	0.00000832	3.135917934
Within Groups	28.764	66	0.43582			
Total	40.9997	68				

However, the comparison between the two human enzymes, AChE and GSK-3β, yielded a mean difference of -0.36652174 and was not statistically significant (p = 0.061210661) (Table 8).

Table 6: T-Test: Two-Sample Assuming Unequal Variances

	AChE (6G1U)	**GSK3 receptor (1Q5K)**
Mean	8.710434783	-8.343913043
Variance	0.237558893	0.591333992
Observations	23	23
Hypothesized Mean Difference	0	
df	37	
t Stat	-1.930698462	
P(T<=t) one-tail	0.03060533	
t Critical one-tail	1.68709362	
P(T<=t) two-tail	0.061210661	
t Critical two-tail	2.026192463	

This indicated that while the ligands interacted more strongly with AChE and GSK-3β than with the quorum sensing bacteria target (4K3B), the strength of their interaction with AChE and GSK-3β is statistically indistinguishable (Table 5). The findings of this study demonstrate a clear and statistically significant selectivity profile for the analyzed ligands. The initial ANOVA test confirmed that the ligands do not interact with the three protein targets uniformly (p = 0.00000832). The subsequent post-hoc analysis provided insightful details into this selectivity, suggesting a preferential interaction with AChE and GSK-3β, which are involved in neurological and oncological pathways, over a critical bacterial protein.

The results of this study offer insight into the potential antifouling mechanism of the analyzed ligands, suggesting a targeted, non-biocidal approach rather than broad toxicity. Modern antifouling research aims to identify compounds that interfere with specific biological processes in fouling organisms, and the present *in-silico* analysis indicates that this chemical scaffold is well-suited for this purpose, primarily by targeting key pathways in macrofouling invertebrates.

A critical finding from the computational analysis is the ligands' significantly weaker interaction with the bacterial protein BamA (4K3B) compared to the eukaryotic enzymes. BamA is essential for outer membrane assembly in Gram-negative bacteria, which are often the primary colonizers that form the microbial biofilm (microfouling) on submerged surfaces. While inhibiting biofilm formation is a valid antifouling strategy, the *in-silico* results suggest that this is not the primary mechanism for these compounds. This hypothesis is strongly supported by experimental evidence. For instance, the studied compounds exhibited only modest antibacterial activity against *Staphylococcus aureus* and *Acinetobacter baumannii* when compared to potent antibacterial like agelasine and the antibiotics tetracycline (Table 1). Furthermore, this observation is consistent with previous reports on related molecules, such as stevensine, which demonstrated weak activity against the key biofilm-forming marine bacterium *Deleya marina.*[16] Therefore, the convergence of computational prediction and experimental data strongly indicates that the primary antifouling action is not through a broad-spectrum antibacterial or biocidal effect. Instead, the clear preferential binding to eukaryotic targets points towards a more specialized mechanism against the latter, more problematic stages of fouling: the settlement and metamorphosis of invertebrate larvae (macrofouling).[40]

The most compelling evidence for a mechanism targeting macrofouling is the highly significant predicted interaction with acetylcholinesterase (AChE) (p = 0.0000004964) (Table 6). In marine invertebrate larvae, such as those of barnacles and polychaetas, the cholinergic nervous system is fundamental for controlling the exploratory behaviour, surface selection, and adhesion processes that precede permanent settlement.[41] As the key regulator of acetylcholine levels, AChE is a critical node in this system. Consequently, AChE inhibition is an established mechanism for non-biocidal antifouling compounds, as it disrupts the larva's ability to sense and respond to settlement cues without causing mortality. To benchmark the potential of our compounds against this target, we compared their predicted binding affinities with those of known standards. Remarkably, stevensine (**3**) and the majority of its derivatives (**3a-3t**) showed predicted binding scores comparable, and in some cases superior (-8.4 to -10.2) kcal/mol, to those of synoxazolidinones A (**5**) and C (**6**) with binding affinities of -8.7 and -8.6 kcal/mol, respectively. Compounds **5** and **6** are not only potent AChE inhibitors but are also validated antifouling agents, proven to likely act through this specific mechanism.[29,30] Therefore, the strong predicted interaction of the stevensine (**3**) chemical class with AChE provides evidence that these ligands likely exert their antifouling effect by interfering with the neural control of larval settlement behaviour.

Table 7: T-Test: Two-Sample Assuming Unequal Variances

	AChE (6G1U)	**Quorum Sensing (4K3B)**
Mean	-8.710434783	-7.692173913
Variance	0.237558893	0.478563241
Observations	23	23
Hypothesized Mean Difference	0	
df	40	
t Stat	-5.770712313	
P(T<=t) one-tail	0.0000004964	
t Critical one-tail	1.683851013	
P(T<=t) two-tail	0.00000099	
t Critical two-tail	2.02107539	

This developmental cascade is tightly controlled by intricate intracellular signaling pathways, including key regulators like GSK-3β, Wnt, and Hedgehog (Hh), alongside TGF-β signaling.[44] GSK-3β is a central player, modulating the canonical Wnt pathway, where its inhibition typically leads to the stabilization of β-catenin and subsequent activation of Wnt target genes crucial for various developmental processes.[45]

Table 8: T-Test: Two-Sample Assuming Unequal Variances

	GSK3-β receptor (1Q5K)	**Quorum Sensing (4K3B)**
Mean	-8.343913043	-7.692173913
Variance	0.591333992	0.478563241
Observations	23	23
Hypothesized Mean Difference	0	
df	44	
t Stat	-3.02180672	
P(T<=t) one-tail	0.002088622	
t Critical one-tail	1.680229977	
P(T<=t) two-tail	0.004177243	
t Critical two-tail	2.015367574	

Concurrently, the Hh signaling pathway is also fundamental for proper larval development and metamorphosis, as evidenced by studies where exposure to the Hh signaling inhibitor cyclopamine impaired larval muscle development, reduced larval swimming activity, and effectively inhibited larval metamorphosis in *M. coruscus*. This cyclopamine-mediated inhibition of Hh signaling directly correlated with reduced expression of four key genes within the Hh pathway (McHh, McPtc, McSmo, and McGl).[46] Therefore, by inhibiting GSK-3β (which critically impacts embryonic development and modulates Wnt signaling) and/or directly interfering with Hh signaling, the test ligands could synergistically disrupt the complex signaling network required for metamorphosis,[47] thereby arresting the larva in its free-swimming stage and preventing its transformation into a hard-fouling adult.

Thus, the present computational analysis gave an important insight into a seemingly undescribed antifouling mechanism. The data suggested these ligands do not primarily act as antibacterial agents against initial biofilm formation. Instead, they appear to function as potent inhibitors of macrofouling through a dual-pronged attack on invertebrate larvae. Additionally, they disrupt the neural processes of settlement by targeting AChE and developmental inhibition. They halt the crucial process of metamorphosis by targeting GSK-3β. This multi-target profile within key eukaryotic pathways is highly desirable for creating effective, environmentally benign antifouling solutions,[48] and provides a strong theoretical basis for future experimental validation using barnacle cyprid settlement and metamorphosis assays.

The analysis also allowed the classification of the computationally-derived library into three distinct functional profiles; GSK-3β-selective, AChE-selective, and dual-inhibitors—indicating the potential of the stevensine scaffold for designing next-generation antifouling agents with tailored mechanisms of action. This approach corroborates with modern antifouling agent discovery where the mechanisms of antifouling compounds become a key biomarker in dictating the optimization of ecofriendly antifoulants.[48]

ISSN 2616-0684 (Print)
ISSN 2616-0692 (Electronic)

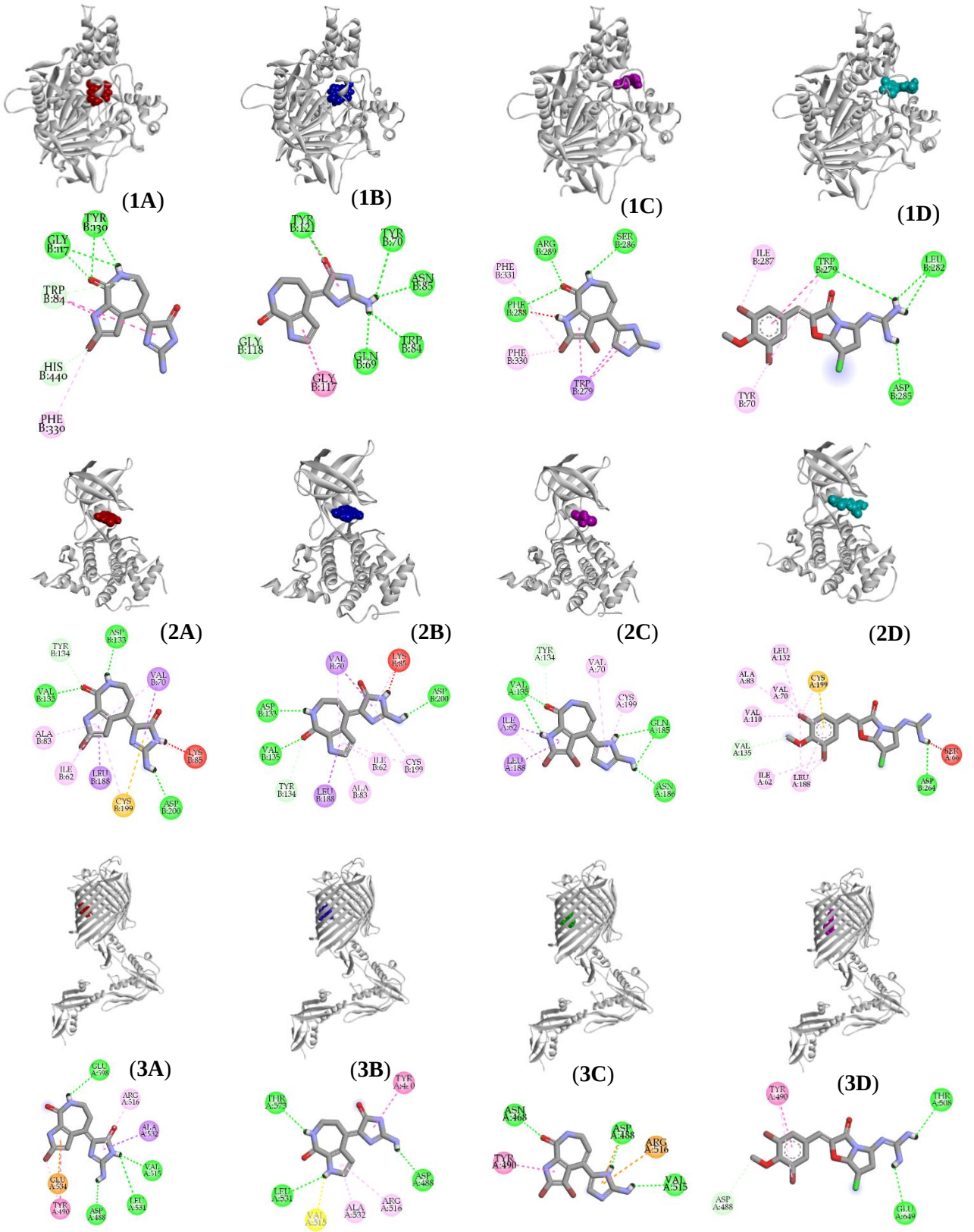

Figure 2: Binding interactions between AChE and hymenialdisine (1A), debromohymenialdisine (1B), stevensine (1C) and synoxalidinone C (1D); GSK-3β and hymenialdisine (2A) debromohymenialdisine (2B), stevensine (2C) and synoxalidinone (2D); QSR and hymenialdisine (3A) debromohymenialdisine (3B), stevensine (3C) and synoxalidinone C (3D).

Furthermore, the significant interaction with Glycogen Synthase Kinase 3 (GSK-3β) (p = 0.004177242) (Table 7) suggests a second, complementary antifouling mechanism that targets critical developmental pathways. GSK-3β is a highly conserved signaling kinase pivotal in regulating cellular development and differentiation.[42] For a swimming larva to become a permanent, sessile fouler, it must undergo a complex and irreversible process of metamorphosis.[43]

ISSN 2616-0684 (Print)
ISSN 2616-0692 (Electronic)

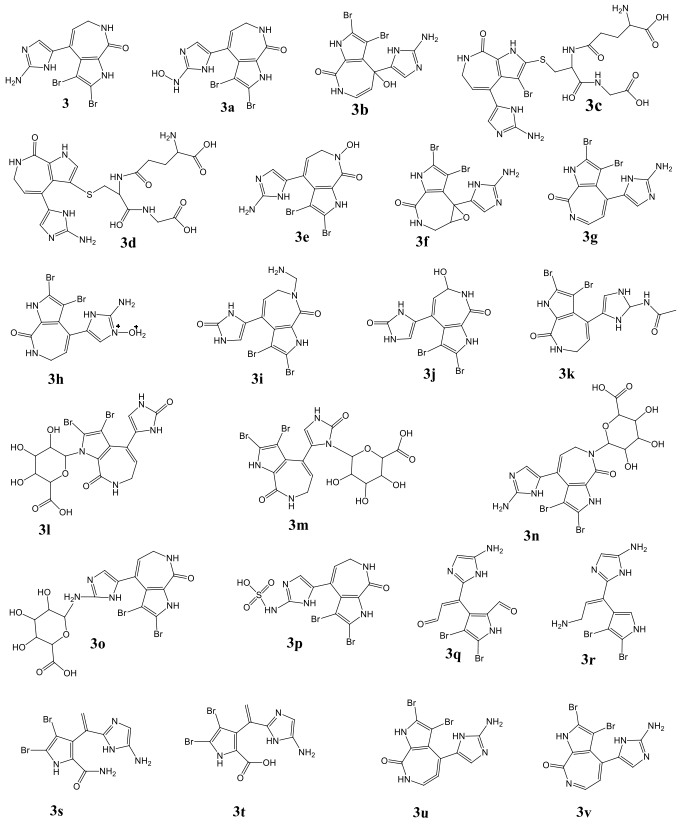

Figure 3: Metabolites generated from MetaTox analysis representing the products of phase I and phase II reactions

Toxicity test

To assess and compare the environmental impact of the compounds, a semi-quantitative method previously developed for risk assessment of triterpenoid sarasinosides was applied.[5] Continuous ecotoxicological data from the EPI Suite™ program (Table 9) were converted into a binary scoring system. Based on established thresholds, each parameter was assigned a score of '1' for a favorable characteristic or '0' for an unfavorable one (Table 10). A total score, representing the proportion of favourable characteristics, was then calculated for each compound, yielding a standardized value between 0 and 1 where higher scores indicate a more favourable environmental profile. To determine if differences between compound groups were statistically significant, Fisher's exact test was performed on a 2 × 2 contingency table comparing the counts of favorable and unfavorable characteristics (Table 11). This approach assumes each parameter contributes equally to the overall environmental risk.

The toxicity test results indicated that most of the stevensine derivatives are potential ecofriendly antifoulants, mainly because of their relatively low risk of bioaccumulation compared to AChE inhibitors and commercial antifouling agents (Table 9). For instance, the octanol-water partition coefficient (Log K_{ow}) values were between -4.54 and 2.05, and the bioconcentration factor (Log BCF) for most derivatives was 3.16 (except for stevensine at 8.25). Additionally, the soil organic carbon-water partitioning coefficient (Log K_{oc}) were between 1.0 and 2.39, with the exception of STV_3 at 3.52. While the Log K_{ow} values were comparable to those of the AChE inhibitors synoxalidinone A (**4**) and C (**5**), which have Log K_{ow} values of 2.05 and 1.59, respectively. Compounds **4** and **5** exhibited high BCF (10.5 and 5.16) and BHL (11 and 4.91) values, exceeding the BCF, Log K_{ow} threshold values of 3.25. Importantly, the commercial antifouling agents Econea® and Selektope® exhibited higher Log K_{ow} (4.69 and 3.83), BCF (575 and 155), and BHL (16.3 and 1.48) values, respectively.

The eco-friendlier profile of the studied bromopyrrole alkaloids is further substantiated by their comparatively low acute toxicity across multiple aquatic trophic levels (Table 9). With the notable exception of the potent antifoulant debromohymenialdisine, the majority of the stevensine derivatives exhibited remarkably high LC_{50}/EC_{50} values. Toxicity thresholds against fish ranged from 3.92×10^{2} to 3.84×10^{8} mg/L, with similarly high values observed for Daphnia (ranging from 2.22×10^{2} to 1.19×10^{8} mg/L) and algae (ranging from 1.59×10^{2} to 7.20×10^{8} mg/L). This low toxicity stands in stark contrast to the commercial antifoulants Econea® and Selektope®, which displayed high toxicity across board, with LC_{50}/EC_{50} values ranging from 10^{-3} to less than 1 mg/L for all three organisms.

Table 9: Toxicity of hymenialdisine (**1**), debromohymenialdisine (**2**), stevensine (**3**), stevensine derivatives (**3c, 3l, 3n-3o, 3t**), synoxalidinones A (**4**) and C (**5**) obtained from EPI Suite™

Compound	Water Solubility (mg/mL)	Fish 96 hr LC_{50} (mg/L)	Daphnid 48 hr LC_{50} (mg/L)	Green Algae 96 hr EC_{50}	Log K_{ow} L/kg (ww)	Log BCF L/kg (ww)	Log BAF L/kg (ww)	BHL	KocWin/Log K_{oc}	Biod. fast	LogP
Hymenialdisine (**1**)	6.9×10^{2}	1.1×10^{3}	6.0×10^{2}	3.4×10^{2}	1.30	3.35	0.94	$2.2x10^{-3}$	2.05	No	0.18
Debromohymenial (**2**)	1.2×10^{-4}	5.4×10^{3}	2.6×10^{3}	1.1×10^{3}	0.41	3.16	0.99	$1.4x10^{-3}$	1.84	No	-0.48
Stevensine (**3**)	8.9×10^{1}	3.9×10^{2}	2.2×10^{2}	1.6×10^{2}	1.89	8.25	6.96	$1.2x10^{-3}$	2.39	No	1.55
STV_3 (**3c**)	4.1×10^{2}	3.8×10^{8}	1.2×10^{8}	7.2×10^{8}	-4,54	3.16	0.89	$2.5x10^{-5}$	3.52	No	-4.16
STV _11 (**3k**)	1.2×10^{2}	2.8×10^{4}	1.3×10^{4}	4.3×10^{3}	-0.11	3.16	0.96	$8.7x10^{-2}$	2.15	No	1.00
STV_10 (**3l**)	3.2×10^{1}	2.9×10^{3}	1.6×10^{3}	8.2×10^{2}	1.10	3.16	1.16	$2.9x10^{-4}$	1.00	No	-0.59
STV_14 (**3n**)	1.6×10^{1}	3.4×10^{5}	1.6×10^{5}	5.3×10^{4}	-0.07	3.16	0.93	$1.8x10^{-3}$	1.00	No	-0.51
STV_15 (**3o**)	7.5×10^{2}	1.9×10^{6}	7.7×10^{5}	1.2×10^{5}	-2.04	3.16	-0.05	$8.5x10^{-4}$	1.00	No	-1.45
STV_20 (**3t**)	2.0×10^{2}	7.5×10^{2}	4.2×10^{2}	2.66×10^{2}	1.53	3.16	0.56	$8.8\ x10^{-3}$	1.38	No	2.03
Synoxalidinone A (**4**)	1.3×10^{1}	8.8×10^{4}	1.1×10^{4}	8.64×10^{3}	2.05	10.5	0.24	1.1×10^{1}	1.95	No	2.50
Synoxalidinone C (**5**)	3.4×10^{1}	1.8×10^{4}	2.010^{4}	1.83×10^{4}	1.59	5.16	1.45	4.9×10^{0}	1.67	No	2.35
Econea (**6**)	3.4×10^{-1}	$3.4x10^{-3}$	2.7×10^{0}	1.49×10^{-2}	4.69	575	3790	1.6×10^{1}	4.54	No	4.89
Selektope (**7**)	2.4×10^{1}	$6.5x10^{-1}$	5.1×10^{-1}	9.50×10^{3}	3.83	155	331	1.4×10^{0}	3.83	No	3.18

ISSN 2616-0684 (Print)
ISSN 2616-0692 (Electronic)

Table 10: Beneficial properties of hymenialdisine (**1**), debromohymenialdisine (**2**), stevensine (**3**), stevensine derivatives (**3c, 3l, 3n-3o, 3t**), synoxalidinones A (**4**) and C (**5**), econea (**6**) and selektope (**7**) calculated using a binary system

Compound	Outcome 1	Outcome 2	Total	*p* values		
				Debromo hymenialdisine	Econea	Selektope
Hymenialdisine (**1**)	7	4	11	0.3108 (2)	0.1984	0.0237*
Debromohymenialdisine (**2**)	10	1	11	-	0.0075*	0.0003***
Stevensine (**3**)	6	5	11	0.1486 (2)	0.3870	0.0635
STV_3 (**3c**)	8	3	11	0.5865 (2)	0.0861	0.0075**
STV _11 (**3k**)	8	3	11	0.5865 (2)	0.0861	0.0075**
STV_10 **(3l)**	8	3	11	0.5865 (2)	0.0861	0.0075**
STV_14 (**3n**)	9	2	11	1.0000 (2)	0.0300*	0.0019***
STV_15 (**3o**)	9	2	11	1.0000 (2)	0.0300*	0.0019***
STV_20 (**3t**)	8	3	11	0.5865 (2)	0.0300*	0.0075**
Synoxalidinone A (**4**)	8	3	11	0.5865 (2)	0.5865	0.0075**
Synoxalidinone C (**5**)	6	5	11	0.1486 (2)	0.1486	0.0635
Econea (**6**)	3	8	11	0.0003***	-	-
Selektope (**7**)	1	10	11	0.0075***	-	-

Table 11: 2 × 2 Contingency Table of Fisher Exact Test among test ligands against reference compounds and commercial antifoulants
Note: *, ** and *** indicate statistically significant, very significant, and extremely significant, respectively

Compound	Water solubility mg/mL	Fish 96 hr LC_{50} mg/L	Daphnid 48 hr LC_{50} mg/L	Green Algae 96 hr EC_{50}	Log K_{ow} L/kg ww	Log BCF L/kg ww	Log BAF L/kg ww	BHL	K_{oc} win/ Log Koc	Biod. fast	LogP	Total score
Hymenialdisine (**1**)	0	1	1	1	1	0	1	1	1	0	0	0.64
Debromohymenialdisine (**2**)	1	1	1	1	1	1	1	1	1	0	1	0.91
Stevensine (**3**)	0	1	1	1	1	0	0	1	1	0	0	0.55
STV_3 (**3c**)	0	1	1	1	1	1	1	1	0	0	1	0.73
STV _11 (**3k**)	0	1	1	1	1	1	1	1	1	0	0	0.73
STV_10 **(3l)**	0	1	1	1	1	1	1	1	1	0	1	0.82
STV_14 (**3n**)	0	1	1	1	1	1	1	1	1	0	1	0.82
STV_15 (**3o**)	0	1	1	1	1	1	1	1	1	0	1	0.82
STV_20 (**3t**)	0	1	1	1	1	1	1	1	1	0	0	0.72
Synoxalidinone A (**4**)	0	1	1	1	1	0	1	0	1	0	0	0.55
Synoxalidinone C (**5**)	0	1	1	1	1	0	1	0	1	0	0	0.55
Econea (**6**)	1	0	1	0	0	0	0	0	1	0	0	0.27
Selektope (**7**)	0	0	0	0	0	0	0	1	0	0	0	0.09

Consequently, the mean toxicity thresholds for the novel stevensine derivatives were several orders of magnitude higher than those of the commercial agents, indicating a significantly reduced risk to non-target aquatic life (Table 9). Furthermore, many derivatives also proved less toxic than the reference AChE inhibitors synoxalidinone A and C. For example, STV_14 exhibited LC_{50} values against fish (3.36×10^5 mg/L) and daphnids (1.57×10^5 mg/L) that were an order of magnitude higher than those of the synoxalidinones (~10^4 mg/L for both organisms).

A holistic comparison using the binary-converted ecotoxicological data further confirms the favourable environmental profile of the stevensine derivatives (Table 10). By synthesizing eleven key parameters into a single total score, this analysis reveals that all novel derivatives demonstrated a markedly superior profile compared to the commercial antifoulants Econea® (Total Score = 0.27) and Selektope® (Total Score = 0.09) (Table 10). Notably, several analogues, particularly STV_10 (**3l**), STV_14 (**3n**), and STV_15 (**3o**), achieved the highest scores among the derivatives at 0.82. While this was slightly lower than the benchmark antifoulant debromohymenialdisine (0.91), these top-performing derivatives, alongside others like STV_20 (**3t**) (0.72), significantly outperformed the other reference compounds, including hymenialdisine (0.64) and the synoxalidinones (0.55). Collectively, this multi-parameter assessment, which goes beyond acute toxicity, strongly supports the potential of the bromopyrrole scaffold for developing safer, more environmentally benign antifouling agents.

The metabolic analysis revealed the formation of four glucuronides and one sulfation product, an observation consistent with the established understanding of Phase II metabolic reactions where glucuronidation frequently dominates due to the broader substrate specificities of UGT enzymes and their involvement in metabolizing a greater proportion of drugs compared to SULT enzymes.[4,5,49–51] While these conjugated metabolites, particularly glucuronides, have traditionally been considered inactive and safe, with minimal impact on therapeutic

ISSN 2616-0684 (Print)
ISSN 2616-0692 (Electronic)

outcomes,[50, 52] the findings for compounds **3l**, **3n**, and **3p**, along with increasing evidence from other studies, demonstrate that these products can exhibit significant biological activity, including enzyme inhibition and ion channel modulation, thereby influencing drug efficacy and safety.[52,53]

To statistically validate the differences in the ecotoxicological profiles among the test compounds, Fisher's exact test was employed (Table 11). The analysis was benchmarked against debromohymenialdisine (**2**), as it achieved the highest total score (Outcome 1 = 10) in our preliminary assessment (Table 11), establishing it as the compound with the most desirable "eco-friendly" characteristics in this study. All other stevensine derivatives, reference compounds, and commercial antifoulants were compared with this benchmark as well as with the commercial products econea (**6**) and selektope (**7**).

The statistical analysis revealed that there was no significant difference between the ecotoxicological profile of the benchmark, debromohymenialdisine (**2**), and several of the newly synthesized stevensine derivatives. Specifically, stevensine (**3**), STV_3 (3c), STV_11 (**3k**), STV_10 (**3l**), and STV_20 (**3t**) all yielded *p*-values greater than 0.05 ($p = 0.1486$ or $p = 0.5865$), indicating statistical parity. This suggests that these derivatives possess an ecotoxicological safety profile of a similarly high standard to the best-identified compound. Likewise, the reference AChE inhibitor synoxazolidinone C (**5**) was also found to be statistically indistinguishable from debromohymenialdisine ($p = 0.1486$).

In comparison against commercial antifoulants, many stevensine derivatives demonstrated statistically superior ecotoxicological profiles. Notably, derivatives STV_14 (**3n**) and STV_15 (**3o**) were not only comparable to hymenialdisine but were also significantly better than econea ($p = 0.0003$) and showed an extremely significant improvement over selektope ($p = 0.0019$). Even the benchmark compound, debromohymenialdisine (**2**), was confirmed to be significantly ($p = 0.0075$) and extremely significantly ($p = 0.0003$) safer than econea (**6**) and selektope (**7**), respectively (Table 11). This highlights a clear and statistically robust advantage, positioning these novel stevensine derivatives as highly promising, next-generation antifoulants with potentially lower environmental impact than existing commercial alternatives.

While derivatives **3c**, **3k**, **3n**, **3o**, and **3t** showed slightly lower values compared to hymenialdisine (0.91), they exhibited a higher total score (0.73-0.82) than the AChE inhibitors synoxalidinone A and C (0.55), and commercial antifoulants such as Econea (0.27) and Selektope (0.09) (Table 11, Figure 4). This suggests their significant beneficial values, particularly when compared to commercial antifoulants. A Python-generated heatmap further revealed their more favourable pharmacological values, positioning them as promising eco-friendly antifouling candidates (Figure 4).

However, for any compound to be effective in a marine coating, it must possess the correct physical properties to ensure its longevity and function. The present analysis revealed that while the novel stevensine derivatives possess favourable ecotoxicological profiles, their practical application is challenged by their high-water solubility. Derivatives such as STV_3, STV_11, STV_15, and STV_20 were highly soluble (119.8 to 748.4 mg/mL), which would likely lead to rapid leaching from a hydrophobic coating, compromising long-term performance.[54,55] In stark contrast, the established antifouling agent debromohymenialdisine exhibited very low water solubility (1.7×10^{-3} mg/mL)—a critical requirement for ensuring a sustained, controlled release into the aquatic environment. Consequently, while promising from an environmental standpoint, the stevensine derivatives would require chemical modification to reduce their solubility before they can be considered viable antifouling agents.

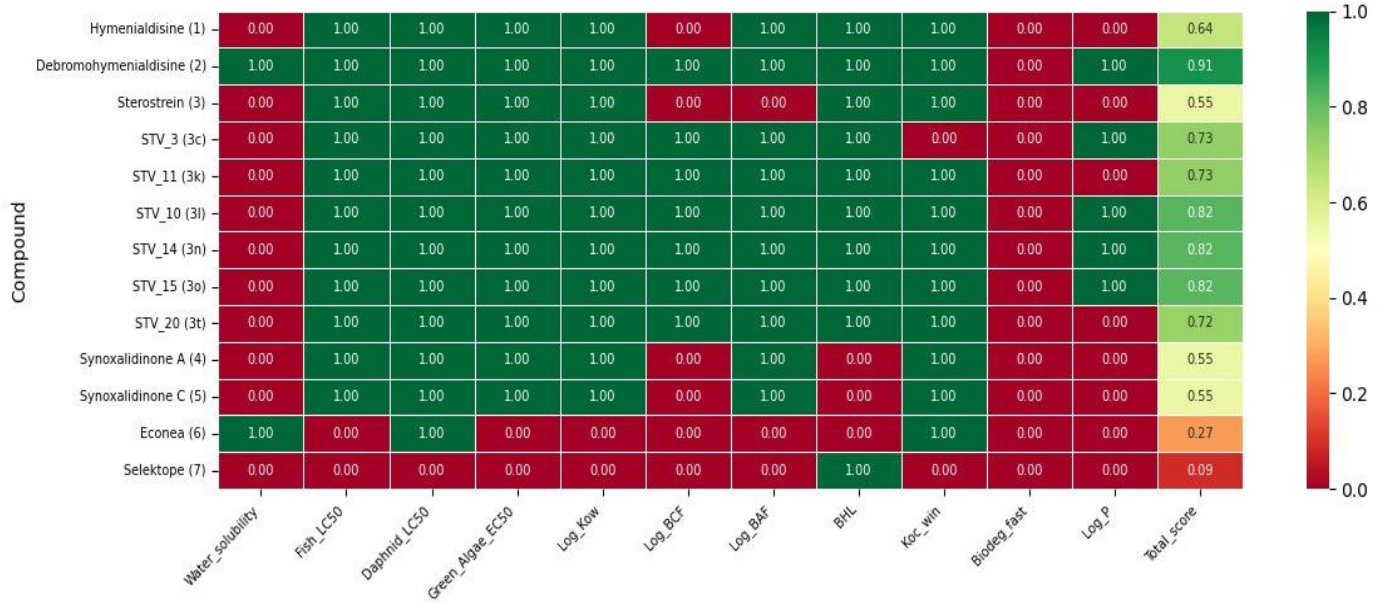

Figure 4: Heatmap of toxicity level of hymenialdisine (**1**), debromohymenialdisine (**2**), stevensine (**3**), stevensine derivatives (3c-3t), synoxalidinone A (**4**), C (**5**), econea (**6**) and selektope (**7**).

These findings highlight a crucial convergence between these fields, as key molecular targets for Alzheimer's disease (AD) are now emerging as viable targets for next-generation antifoulants. This strategy centers on Glycogen Synthase Kinase-3β (GSK-3β) and Acetylcholinesterase (AChE), enzymes central to AD pathology that are now implicated in biofouling processes. The potent, dual inhibition of both AChE and GSK-3β by the stevensine derivatives fits perfectly within this MTDL strategy, aligning with the understanding that the most effective antifouling agents are often those designed to interact with more than one target.[42]

This multi-target potential is reinforced by the distinct binding modes observed. The varied interaction patterns of stevensine (binding to Cys199, Leu188, Val70) versus hymenialdisine and debromohymenialdisine (binding to Ala83, Asp200) within the GSK-3β active site are not anomalous. Rather, they exemplify a cutting-edge trend in drug design, moving beyond traditional ATP-competitive mechanisms to exploit distinct substrate-binding or allosteric sites to achieve greater selectivity.[56] The interaction with Asp200, in particular, has been identified as critical for inhibitor selectivity.[57]

To this end, while the physicochemical properties of the novel stevensine derivatives require optimization for coating applications

particularly for their water solubility, their biological profile is highly significant. They represent a class of compounds that embodies the modern, multi-target design philosophy now central to both advanced therapeutics and the future of sustainable antifouling technologies.

It is worth noting also that this study has several key limitations. Its primary reliance on computational methods means that both the ecotoxicological profiles and the predicted metabolites generated *in silico*, require experimental validation through standardized aquatic toxicity and metabolic assays. Furthermore, a significant hurdle to practical application is the lack of a commercially viable supply chain; while laboratory-scale synthesis of stevensine structure class exists,[58] large-scale production and mariculture of the source sponge remain undeveloped. Finally, the long-term environmental fate and biodegradability of these compounds were not assessed in the marine environment - a critical step needed to fully confirm their "ecofriendly" designation.

Future work will prioritize the isolation of pure stevensine and its derivatives to experimentally validate their antifouling activity and *in silico* toxicity predictions. Concurrently, mechanistic studies, including biochemical assays and molecular modeling will be conducted to confirm the inhibition of AChE and GSK-3β and explore potential allosteric binding sites. This exploration may lead to the development of new antifoulants. In fact, the discovery of new allosteric sites for both GSK-3β and AChE has been reported as a promising avenue for identifying effective modulators. This is partly due to their moderate and tunable inhibition, which is ideal for both AChE and GSK-3β because of their involvement in multiple pathways.[34,59,60] Such discoveries are likely to contribute to the identification of new eco-friendly antifouling candidates. However, despite considerable research efforts, only one allosteric GSK-3β inhibitor has reached clinical trials. To address the challenges of scalability and solubility, a subsequent structure-activity relationship (SAR) study will be employed. This will involve using computational tools to identify the core pharmacophore, guiding the synthesis of simplified, more accessible analogues that retain biological efficacy while possessing superior physicochemical and environmental profiles.

Conclusion

In summary, this *in-silico* investigation has successfully identified stevensine and its related bromopyrrole alkaloids as promising candidates for a new class of environmentally sustainable antifouling agents. Through a comprehensive computational analysis, it has been demonstrated that these compounds possess a predicted ecotoxicological profile far superior to that of current commercial antifoulants. Furthermore, molecular docking studies provided a strong mechanistic hypothesis for their efficacy, suggesting a multi-target mechanism via the dual inhibition of acetylcholinesterase and GSK-3β. By integrating predictive toxicity, bioaccumulation potential, and mechanistic insights, this study provides a robust, data-driven foundation for their advancement. While we acknowledge that these computational findings must be contextualized, particularly regarding selectivity when compared to highly optimized agents like Selektope, this work establishes these natural alkaloids as leading candidates worthy of experimental validation and synthetic optimization. The path forward now lies in translating these compelling computational predictions into tangible, next-generation antifouling solutions.

Conflict of Interest

The authors declare no conflict of interest.

Author's Declaration

The authors hereby declare that the work presented in this article is original and that any liability for claims relating to the content of this article will be borne by them.

Acknowledgments

The authors are grateful to the Indonesian Ministry of Higher Education, Science, and Technology for financial support (No. 182/C3/DT.05.00/PL-BATCH II/2025).

References

1. Qian PY, Li Z, Xu Y. Marine Natural Products as Antifouling Agents. Springer, Berlin; 2015.
2. Gaudêncio SP and Pereira F. Predicting Antifouling Activity and Acetylcholinesterase Inhibition of Marine-Derived Compounds Using a Computer-Aided Drug Design Approach. Mar Drugs. 2022; 20(2):129. Doi:10.3390/md20020129.
3. Gomez-Banderas J. Marine Natural Products: A Promising Source of Environmentally Friendly Antifouling Agents for The Maritime Industries. Front Mar Sci. 2022; 9:858757. Doi:10.3389/fmars.2022.858757.
4. Balansa W, Riyanti, Manurung UN, Tomasoa AM, Hanif N, Rieuwpassa FJ, Schäberle TF. Sponge-Based Ecofriendly Antifouling: Field Study on Nets, Molecular Docking with Agelasine Alkaloids. Trop J Nat Prod Res. 2024; 8(1):5913–5924.
5. Ghattavi S, Homaei A, Fernandes P. Marine Natural Products for Biofouling Elimination in Marine Environments. Biocat. Agr. Biotech. 2024; 61, 103385. Doi: 10.1016/j.bcab.2024.10338
6. Balansa W, Riyanti R, Rieuwpassa FJ, Hanif N. Harnessing Ecofriendly Antifouling of Agelasine Alkaloids. Kamija Aquat. 2025. 143 p.
7. Balansa W, Riyanti R, Balansa KH, Hanif N. Harnessing the Ecofriendly Antifouling Potential of Agelasine Alkaloids Through MetaTox Analysis and Computational Studies. Trop J Nat Prod Res. 2025; 9(1):329–340. https://doi.org/10.26538/tjnpr/v9i1.42
8. Akunuri R, Vadakattu M, Bujji S, Veerareddy V, Madhavi YV, Nanduri S. Fused-azepinones: Emerging Scaffolds of Medicinal Importance. Eur J Med Chem. 2021; 220:113445. Doi: 10.1016/j.ejmech.2021.113445.
9. Balansa W, Riyanti, Patras MA, Balansa KH, Hanif N, Rieuwpassa FJ, Hill M, Schäberle TF. Harnessing the Metabolites from the Marine Sponge *Melophlus sarasinorum* for the Discovery of Eco-friendly Antifoulants. Biodiversitas. 2025; 26(4):1590–1606.
10. Ivanchina NV and Kalinin VI. Triterpene and Steroid Glycosides from Marine Sponges (Porifera, Demospongiae): Structures, Taxonomical Distribution, Biological Activities. Molecules. 2023; 28(6):2503. Doi:10.3390/molecules28062503.
11. Austin P, Freeman SA, Gray CA, Gold MR, Vogl AW, Andersen RJ, Roberge M, Roskelley CD. The Invasion Inhibitor Sarasinoside A1 Reverses Mesenchymal Tumor Transformation in an E-cadherin-Independent Manner. Mol Cancer Res. 2013; 11:530–540. Doi: 10.1158/1541-7786.MCR-12-0385
12. Pérez-Aguilar B, Marquardt JU, Muñoz-Delgado E, López-Durán RM, Gutiérrez-Ruiz MC, Gomez-Quiroz LE. Changes in the Acetylcholinesterase Enzymatic Activity in Tumor Development and Progression. Cancers (Basel). 2023; 15:4629. Doi:10.3390/cancers15184629.
13. Dan, QF, Qiu Y, Wang W, Wang X, Ouyang PG, Ke CH. Antifouling Activities of Hymenialdisine and Debromohymenialdisine from the Sponge *Axinella* sp., Inter. Biodeter. Biodeg. 2013, 85, 359-364. Doi.org/10.1016/j.ibiod.2013.08.014.
14. Chandramouli KH, Qian PY, Ravasi T. Proteomics Insights: Proteins Related to Larval Attachment and Metamorphosis of Marine Invertebrates. Front Mar Sci. 2014; 1:52. Doi:10.3389/fmars.2014.00052.
15. Wilson DM, Puyana M, Fenical W, Pawlik JR. Chemical Defense of the Caribbean Reef Sponge *Axinella corrugata* Against Predatory Fishes. J Chem Ecol. 1999; 25:2811–2823.
16. Newbold RW, Jensen PR, Fenical W, Pawlik JR. Antimicrobial Activity of Caribbean Sponge Extracts. Aquat Microb Ecol. 1999; 19:279–284.
17. Vrabec R, Blunden G, Cahlíková L. Natural Alkaloids as Multi-Target Compounds Towards Factors Implicated in Alzheimer's Disease. Int J Mol Sci. 2023; 24(5):4399. Doi:10.3390/ijms24054399.
18. Arabshahi HJ, Trobec T, Foulon V, Hellio C, Frangež R, Sepčić K, Cahill P, Svenson J. Using Virtual AChE Homology Screening to Identify Small Molecules with the Ability to Inhibit Marine

Biofouling. Front Mar Sci. 2021; 8:762287. Doi:10.3389/fmars.2021.762287.
19. Dallakyan S, Olson AJ. Small-Molecule Library Screening by Docking with PyRx. In: Hempel JE, Williams CH, Hong CC, editors. Chemical Biology: Methods and Protocols. Springer New York, New York, NY; 2015. 243–250 p.
20. Card ML, Gomez-Alvarez V, Lee WH, Lynch DG, Orentas NS, Lee MT, Wong EM, Boethling RS. History of EPI SuiteTM and Future Perspectives on Chemical Property Estimation in US Toxic Substances Control Act New Chemical Risk Assessments. Environ Sci Proc Impacts. 2017; 19(3):203–212. Doi:10.1039/c7em00064b
21. Balansa W, Wodi SIM, Rieuwpassa FJ, Ijong FG. Agelasines B, D and Antimicrobial Extract of a Marine Sponge *Agelas* sp. From Tahuna Bay, Sangihe Islands, Indonesia. Biodiversitas. 2020; 21(2):699–706. Doi:10.13057/biodiv/d210236.
22. Rudik A, Bezhentsev V, Dmitriev A, Lagunin A, Filimonov D, Poroikov V. Metatox - Web Application for Generation of Metabolic Pathways and Toxicity Estimation. J Bioinform Comput Biol. 2019; 19:19400018. Doi:10.1142/S0219720019400018.
23. Atkins P and Paula J de. Atkins' Physical Chemistry. 10th ed. Oxford University Press, New York; 2014.
24. Riyanti, Marner M, Hartwig C, Patras MA, Wodi SIM, Rieuwpassa FJ, Ijong FG, Balansa W, Schäberle TF. Sustainable Low-Volume Analysis of Environmental Samples by Semi-Automated Prioritization of Extracts for Natural Product Research (SeaPEPR). Mar Drugs. 2020; 18(12):649. Doi:10.3390/md18120649.
25. Peng Q, Tang X, Dong W, Sun N, Yuan W. A Review of Biofilm Formation of *Staphylococcus aureus* and Its Regulation Mechanism. Antibiotics. 2023; 12(1):12. Doi:10.3390/antibiotics12010012.
26. Jia Z. Antifouling Strategies-Interference with Bacterial Adhesion. Focus on Bacterial Biofilms. InTechOpen; 2022. Doi:10.5772/intechopen.102965.
27. Mishra A, Aggarwal A, Khan F. Medical Device-Associated Infections Caused by Biofilm-Forming Microbial Pathogens and Controlling Strategies. Antibiotics. 2024; 13(7):623. Doi:10.3390/antibiotics13070623.
28. Patra A, Das J, Agrawal NR, Kushwaha GS, Ghosh M, Son YO. Marine Antimicrobial Peptides-Based Strategies for Tackling Bacterial Biofilm and Biofouling Challenges. Molecules. 2022; 27(21):7546. Doi:10.3390/molecules27217546.
29. Trepos R, Cervin G, Hellio C, Pavia H, Stensen W, Stensvåg K, Svendsen JS, Haug T, Svenson J. Antifouling Compounds from The Sub-Arctic Ascidian *Synoicum pulmonaria*: Synoxazolidinones A and C, Pulmonarins A and B, and Synthetic Analogues. J Nat Prod. 2014; 77:2105–2113. Doi: 10.1021/np5005032
30. Tadesse M, Svenson J, Sepčić K, Trembleau L, Engqvist M, Andersen JH, Jaspars M, Stensvåg K, Haug T. Isolation and Synthesis of Pulmonarins A and B, Acetylcholinesterase Inhibitors from The Colonial Ascidian *Synoicum pulmonaria*. J Nat Prod. 2014; 77:364–369. Doi: 10.1021/np401002s
31. Pérez-Aguilar B, Marquardt JU, Muñoz-Delgado E, López-Durán RM, Gutiérrez-Ruiz MC, Gomez-Quiroz LE, Gómez-Olivares JL. Changes in the Acetylcholinesterase Enzymatic Activity in Tumor Development and Progression. Cancers (Basel). 2023; 15(18):4629. Doi: 10.3390/cancers15184629.
32. Pandey MK and DeGrado TR. Glycogen Synthase Kinase-3 (GSK-3)-Targeted Therapy and Imaging. Theranostics. 2016; 6:571–593. Doi: 10.7150/thno.14334
33. Kalinin VI, Ivanchina NV, Krasokhin VB, Makarieva TN, Stonik VA. Glycosides from Marine Sponges (Porifera, Demospongiae): Structures, Taxonomical Distribution, Biological Activities and Biological Roles. Mar Drugs. 2012; 10:1671–1710. Doi.org/10.3390/md10081671.
34. Luque FJ and Muñoz-Torrero D. Acetylcholinesterase: A Versatile Template to Coin Potent Modulators of Multiple Therapeutic Targets. Acc Chem Res. 2023; 56(19):2775–2787. Doi:10.1021/acs.accounts.3c00617.
35. Qian PY, Chen L, Xu Y. Mini-review: Molecular Mechanisms of Antifouling Compounds. Biofouling. 2013; 29:381–400. Doi: 10.1080/08927014.2013.776546
36. Qiu Q, Gu Y, Ren Y, Ding H, Hu C, Wu D, Mou J, Wu Z, Dai D. Research Progress on Eco-friendly Natural Antifouling Agents and Their Antifouling Mechanisms. Chem Eng J. 2024; 495:153638. Doi:10.1016/j.cej.2024.153638
37. Thapa R, Gupta G, Bhat AA, Kumar S, Khan S, Alqahtani YS, Sharma V, Albadawi DA. A Review of Glycogen Synthase Kinase-3 (GSK3) Inhibitors for Cancers Therapies. Int J Biol Macromol. 2023; 253:127375. Doi: 10.1016/j.ijbiomac.2023.127375.
38. An J, Xie HQ, Yan Z, Chen X, Zhu R, Yang G, Xu L, Kovarik Z, Keung Tsim KW. Pan-cancer Analysis of Acetylcholinesterase (AChE) Expression by a Data-Driven Approach: Future Directions of AChE in Cancer Neuroscience. Chem Biol Interact. 2025; 3:111647. Doi:10.1016/j.cbi.2025.111647.
39. Storek KM and Rutherford ST. Inhibitors Targeting BamA in Gram-Negative Bacteria. Biochim Biophys Acta Mol Cell Res. 2024; 1871(1):119609. Doi:10.1016/j.bbamcr.2023.119609.
40. Antunes J, Leão P, Vasconcelos V. Marine Biofilms: Diversity of Communities and of Chemical Cues. Environ Microbiol Rep. 2019; 11:287–305. Doi: 10.1111/1758-2229.12694.
41. Faimali M, Falugi C, Gallus L, Piazza V, Tagliafierro G. Involvement of Acetyl Choline in Settlement of *Balanus amphitrite*. Biofouling. 2003; 19:213–220. Doi.org/10.1080/0892701021000044228
42. Cahill, P. L., Moodie, L. W. K., Hertzer, C., Pinori, E., Pavia, H., Hellio, C., Brimble, M. A., & Svenson, J. Nature-inspired Solutions for Marine Biofouling: From Natural Products to Biomimetic Coatings. Acc. Chem. Res., 2024, 57(3), 399–412. https://doi.org/10.1021/acs.accounts.3c00733.
43. Whalan S, Abdul Wahab MA, Sprungala S, Poole AJ, De Nys R. Larval Settlement: The Role of Surface Topography for Sessile Coral Reef Invertebrates. PLoS One. 2015; 10(3):e0117675. Doi:10.1371/journal.pone.0117675.
44. Borisenko I, Podgornaya OI, Ereskovsky AV. Chapter Twelve - From Traveler to Homebody: Which Signaling Mechanisms Sponge Larvae Use to Become Adult Sponges? Adv Protein Chem Struct Biol. 2019; 117:421–449. Doi: 10.1016/bs.apcsb.2019.02.002
45. Shimizu M, Shibuya H. GSK3β Regulates a Novel β-Catenin Degradation Pathway via the GID Complex in Wnt Signaling. Gen Cell. 2025 Nov;30(6):e70068. Doi:10.1111/gtc.70068.
46. Tang Y, Wang YQ, Ni JY, Lin YT, Li YF. Hedgehog Signaling Is Required for Larval Muscle Development and Larval Metamorphosis of The Mussel *Mytilus coruscus*. Dev Biol. 2024; 512:57–69. Doi: 10.1016/j.ydbio.2024.05.007
47. Wu D and Pan W. GSK3: A Multifaceted Kinase in Wnt Signaling. Trends Biochem Sci. 2010; 35:161–168. Doi: 10.1016/j.tibs.2009.10.002
48. Chen L, Qian PY. Review on Molecular Mechanisms of Antifouling Compounds: An Update since 2012. Mar Drugs. 2017. 28;15(9):264. Doi: 10.3390/md15090264.
49. Cerny MA. Prevalence of Non-cytochrome P450- Mediated Metabolism in Food and Drug Administration Approved Oral and Intravenous Drugs: 2006-2015. Drug Metab Dispos. 2016; 44:1246–1252. Doi: 10.1124/dmd.116.070763
50. Järvinen E, Deng F, Kiander W, Sinokki A, Kidron H, Sjöstedt N. The Role of Uptake and Efflux Transporters in the Disposition of Glucuronide and Sulfate Conjugates. Front Pharmacol. 2022; 12:802539. Doi:10.3389/fphar.2021.802539.
51. Yang G, Ge S, Singh R, Basu S, Shatzer K, Zen M, Liu J, Tu Y, Zhang C, Wei J, Shi J, Zhu L, Liu Z, Wang Y, Gao S, Hu M. Glucuronidation: Driving Factors and Their Impact on Glucuronide Disposition. Drug Metab Rev. 2017; 49(2):105-138. Doi: 10.1080/03602532.2017.1293682.
52. Tornio A, Filppula AM, Kailari O, Neuvonen M, Nyrönen TH, Tapaninen T, Neuvonen PJ, Niemi M, Backman JT. Glucuronidation Converts Clopidogrel To a Strong Time-Dependent Inhibitor of CYP2C8: A Phase II Metabolite as a

Perpetrator of Drug–Drug Interactions. Clin Pharmacol Ther. 2014; 96:498–507. Doi: 10.1038/clpt.2014.141
53. Vitku J, Hill M, Kolatorova L, Kubala Havrdova E, Kancheva R. Steroid Sulfation in Neurodegenerative Diseases. Front Mol Biosci. 2022; 9:1–16. Doi:10.3389/fmolb.2022.846511.
54. Vilas-Boas C, Silva ER, Resende D, Pereira B, Sousa G, Pinto M, Almeida JR, Correia-da-Silva M, Sousa E. 3,4-Dioxygenated Xanthones as Antifouling Additives for Marine Coatings: *In silico* Studies, Seawater Solubility, Degradability, Leaching, and Antifouling Performance. Environ Sci Pollut Res. 2023; 30:68987–68997. Doi : 10.1007/s11356-023-26899-1.
55. Vilas-Boas C, Neves AR, Carvalhal F, Sousa E. Multidimensional Characterization of a New Antifouling Xanthone: Structure-activity Relationship, Environmental Compatibility, and Immobilization in Marine Coatings. Ecotoxicol Environ Saf. 2021; 228:112970. Doi : 10.1016/j.ecoenv.2021.112970
56. Balboni B, Tripathi SK, Veronesi M, Russo D, Penna I, Giabbai B, Bandiera T, Storici P, Girotto S, Cavalli A. Identification of Novel GSK-3β Hits Using Competitive Biophysical Assays. Int J Mol Sci. 2022; 23(7):3856. Doi:10.3390/ijms23073856.
57. Benghanem S, Mesli F, Zohra HAF, Nacereddine C, Hadjer C, Abdellatif M. Discovery of Novel and Highly Potential Inhibitors of Glycogen Synthase Kinase 3-beta (GSK-3β) Through Structure-based Pharmacophore Modeling, Virtual Computational Screening, Docking and *In silico* ADMET Analysis. J Biomol Struct Dyn. 2024; 42:7091–7106. Doi: 10.1080/07391102.2023.2238062.
58. Xu Y, Yakushijin K and Horne DA. Synthesis of C11N5 Marine Sponge Alkaloids: (±)-Hymenin, Stevensine, Hymenialdisine, and Debromohymenialdisine. J Org Chem. 1997; 62:456–464. Doi: 10.1021/jo9619746.
59. Roca C, Requena C, Sebastián-Pérez V, Malhotra S, Radoux C, Pérez C, Martinez A, Antonio Páez J, Blundell TL, Campillo NE. Identification of New Allosteric Sites and Modulators of AChE Through Computational and Experimental Tools. J Enzyme Inhib Med Chem. 2018; 33:1034–1047. Doi: 10.1080/14756366.2018.1476502.
60. Balboni B, Masi M, Rocchia W, Girotto S, Cavalli A. GSK-3β Allosteric Inhibition: A Dead End or a New Pharmacological Frontier? Int J Mol Sci. 2023; 24(8):7541. Doi:10.3390/ijms24087541.
61. Hooper, J. N. A., & Van Soest, R. W. M. 2002. Systema Porifera: A Guide to the Supraspecific Classification of the Phylum Porifera. 1707.
62. Rieuwpassa, FJ., Tomasoa AM, Palawe JF, Rieuwpassa F, Mege RA, Balansa W. A New and Practical Method for Measuring Sponge Spicules. J. Ilm. Platax, 2023, 11(2), 322-332. Doi.org/10.35800/jip.v11i2.47882.